



Magma ocean fractional crystallization and cumulate overturn in terrestrial planets: Implications for Mars

Linda T. ELKINS-TANTON,* E. M. PARMENTIER, and P. C. HESS

Brown University, Department of Geological Sciences, Providence, Rhode Island 02912, USA

*Corresponding author. E-mail: Linda_Elkins_Tanton@brown.edu

(Received 3 February 2002; revision accepted 31 October 2003)

Abstract—Crystallization of a magma ocean on a large terrestrial planet that is significantly melted by the energy of accretion may lead to an unstable cumulate density stratification, which may overturn to a stable configuration. Overturn of the initially unstable stratification may produce an early basaltic crust and differentiated mantle reservoirs. Such a stable compositional stratification can have important implications for the planet's subsequent evolution by delaying or suppressing thermal convection and by influencing the distribution of radiogenic heat sources. We use simple models for fractional crystallization of a martian magma ocean, and calculate the densities of the resulting cumulates. While the simple models presented do not include all relevant physical processes, they are able to describe to first order a number of aspects of martian evolution. The models describe the creation of magma source regions that differentiated early in the history of Mars, and present the possibility of an early, brief magnetic field initiated by cold overturned cumulates falling to the core-mantle boundary. In a model that includes the density inversion at about 7.5 GPa, where olivine and pyroxene float in the remaining magma ocean liquids while garnet sinks, cumulate overturn sequesters alumina in the deep martian interior. The ages and compositions of source regions are consistent with SNC meteorite data.

INTRODUCTION

Significant and perhaps complete melting of the large terrestrial planets is expected due to the conversion of kinetic energy to heat during accretion of planetesimals (e.g., Halliday et al. 2001). The processes of solidification of the magma ocean determine the initial planetary compositional differentiation. The stability of this differentiation has significance for magmatic source regions, convective instability, and magnetic field generation. Although progress on the dynamical problem of magma ocean crystallization has been made by a number of workers (e.g., Tonks and Melosh 1990; Davies 1990; Franck 1992; Morse 1993; Solomatov and Stevenson 1993a, b; Abe 1993, 1997; Solomatov 2000), the dynamic and compositional consequences of crystallizing a magma ocean have not previously been investigated specifically for Mars. Previous studies have determined likely bulk compositions for silicate Mars (e.g., Dreibus and Wänke 1985; Bertka and Fei 1997) and have modeled the expected phase assemblages in the mantle both experimentally and theoretically (e.g., Longhi et al. 1992; Bertka and Fei 1997, 1998a, b). These studies have made significant progress in constraining the depth of the core-mantle boundary and in

defining density profiles that are consistent with the moment-of-inertia factor of the present planet.

The existence of an early magma ocean in Mars is supported by ^{182}W and ^{142}Nd anomalies that date the fractionation of the core and mantle to within 13 ± 2 Myr of the origin of the solar system (Kleine et al. 2002; Blichert-Toft et al. 1999; Lee and Halliday 1995). The extreme ϵ_{Nd} values and presence of ^{142}Nd anomalies indicate that the SNC meteorite source reservoirs differentiated very early in Mars' history and have remained separate (Jones 1986; Borg et al. 1997). Brandon et al. (2000) have also correlated the ^{182}W and ^{142}Nd anomalies with Re-Os systematics, arguing that the isotopic composition of the martian meteorites was set in the earliest differentiation history of Mars, indicating that crystallization of a martian magma ocean postdated earliest core formation. Correlations of ϵ_{W} with ϵ_{Nd} in martian samples are also suggested by Righter and Shearer (2003) to be the result of early clinopyroxene or garnet fractionation in the martian mantle, a scenario consistent with solidification of a magma ocean. Note, however, that Righter et al. (1998) determined that martian Ni, Co, Mo, W, P, and Re abundances estimated from melt inclusions in martian meteorites are consistent with a hot magma ocean of only a 700 to 800 km depth.

The preservation of whole rock Rb-Sr isochrons and ^{182}W and ^{142}Nd anomalies are also evidence that there has been little or no crustal recycling since magma ocean solidification (Hess 2002; Blichert-Toft et al. 1999). Blichert-Toft et al. (1999) narrowed the age of differentiation to perhaps the first 100 Myr after accretion, and Shih et al. (1999) concluded that early differentiation occurred by 4.558 Ga, or less than 10 Myr after accretion.

Though the martian mantle differentiated very early, and little crustal recycling has occurred since, martian magmatism has been long-lived. The oldest known martian rocks are crustal rocks, such as Allan Hills 84001, which has an age of 4.5 Ga. From the SNC meteorites, evidence exists for magmatism from 1.3 Ga to as recently as 170 Myr before the present (e.g., Blichert-Toft et al. 1999; Shih et al. 1999; Borg et al. 2002; Herd et al. 2002).

The extent to which the terrestrial planets melted during accretion has not been determined conclusively, even in the case of the Moon, with its long-standing magma ocean hypothesis for the formation of the anorthositic highlands (e.g., Wood et al. 1970). Estimates for the depth of the magma ocean on the Earth, Mars, and the Moon vary widely, and workers have suggested the possibility of laterally heterogeneous magma ponds rather than a homogeneous magma ocean (e.g., Solomatov 2000). For the Moon, the body with arguably the best evidence for a magma ocean, depth estimates range from 250 to 1000 km depth (Warren 1985). Melting requires high temperatures to be created by energetic accretion and to be maintained by either or both an insulating atmosphere or rapid accretion (Abe and Matsui 1985). In the case of the Earth, its relatively large size and the likelihood of a Mars-sized impactor creating the Moon (e.g., Canup and Asphaug 2001) make a complete melting early in Earth history relatively likely. Mars' smaller size limits its heating by accretion, but the possibility of early atmosphere formation by degassing and its recently determined rapid accretion raise the possibility of complete melting. The brief interval (13 ± 2 Ma; Kleine et al. 2002) over which Mars was accreted from planetesimals makes complete melting more likely. Complete melting of the early planet is, in any case, an end member possibility for the effects of accretionary heat on planetary formation and is the focus of this study.

The SNC meteorite compositions indicate an iron-rich, alumina-poor source, compared to the Earth's mantle (Longhi et al. 1992). Isotopic characteristics indicate that the nakhlites and Chassigny came from an incompatible-element-depleted source and that Elephant Moraine A79001, Los Angeles, Zagami, and Shergotty all came from an incompatible-element-enriched source (Blichert-Toft et al. 1999; Herd et al. 2002; Borg et al. 2002). Borg et al. (2002) argues, on the basis of Nd isotopes, for 2 ancient sources that mixed to make the shergottites. Thus, at least 3 isotopically distinct reservoirs have been inferred: 2 incompatible-element-enriched sources (for example, very late-stage magma ocean cumulates or

solids produced by crystallizing a second-stage melting event) and at least 1 incompatible-element-depleted source (such as magma ocean cumulates).

Though the current magnetic field of Mars is about 4 orders of magnitude less than Earth's, indicating no currently active core dynamo, patches of crustal rocks on Mars are magnetized more strongly than the Earth's crust (Acuña et al. 1999; Connerney et al. 1999). The intensity of the magnetization, combined with its existence principally in ancient crust, may imply that Mars had a vigorous core dynamo only briefly in its early history (e.g., Stevenson 2001). Planetary magnetic fields are widely hypothesized to be created by convective motions driven by super-adiabatic heat flow out of a liquid metal outer core (e.g., Verhoogen 1961; Braginsky 1975). Mantle dynamics may have controlled the creation and destruction of the core-mantle temperature gradient and the resulting heat flux necessary to create a strong magnetic field early in Mars' history.

The goals of this study are to create a simple model for crystallization of a martian magma ocean and assess the outcome of overturn due to density instability (Hess and Parmentier 2001). The results of these crystallization and overturn models will be presented in terms of phases, compositions, and density and temperature profiles. We will investigate the possibility that such crystallization and overturn can explain aspects of the martian magnetic field and can reproduce the compositional characteristics predicted for the source regions of the martian igneous meteorites.

MODELS

We assume that the planet is initially entirely above its liquidus. Vigorous convection in the low viscosity liquid magma ocean, above a potential temperature of about 2000°C, is assumed to result in an adiabatic variation of temperature with depth and a homogeneously mixed liquid composition. The thermal structure implied by these idealizations is illustrated in Fig. 1. The solidus (Longhi et al. 1992) was calculated for the bulk martian mantle composition of Dreibus and Wänke (1985) and is consistent with our assumed bulk composition discussed later. Figure 1 also shows approximate adiabats for liquid and for material lying between the solidus and liquidus. As the magma ocean crystallizes in our model, each package is assumed to crystallize at the solidus and retain its solidus temperature as the rest of the magma ocean crystallizes. This assumes that solidification occurs rapidly compared to heat conduction or flow in the solid.

As the liquid magma ocean cools by the loss of heat convected to the surface of the planet, the adiabat intersects the liquidus at the bottom of the mantle. This adiabatic thermal structure ignores the possibility of developing a compositionally layered liquid and complexities such as separately convecting liquid layers. As the ocean continues to

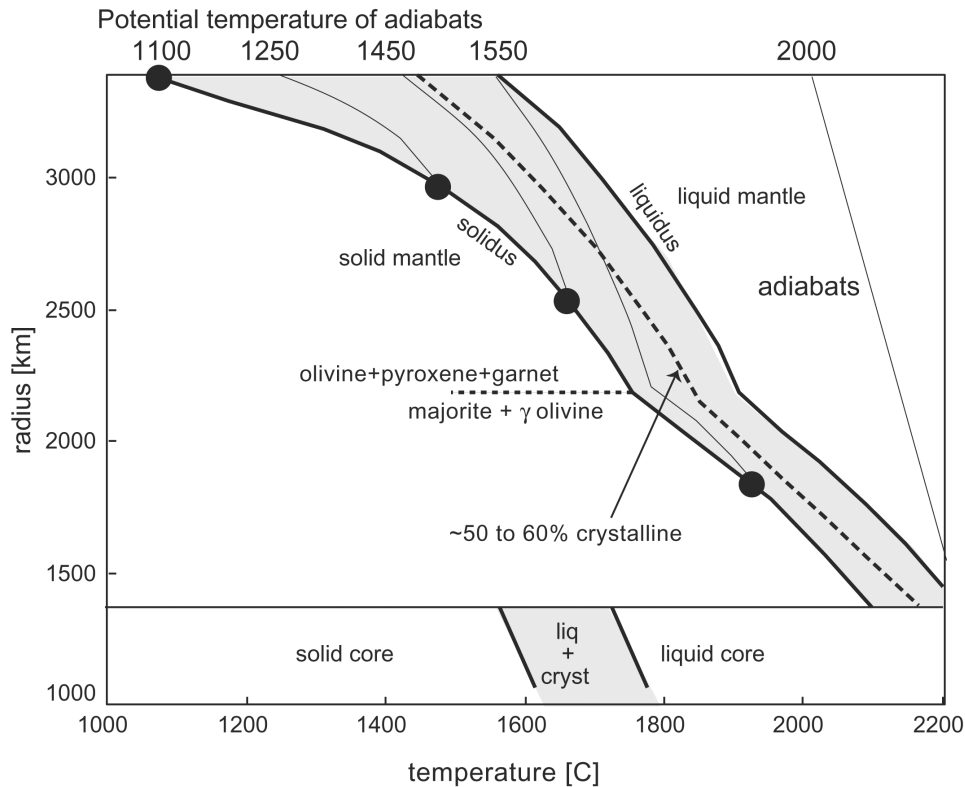


Fig. 1. Solidus and liquidus for martian core and mantle compositions from Longhi et al. (1992), with approximate adiabats (thin lines) for the liquid and partly crystalline magma oceans drawn in to demonstrate the possibility of crystalline, crystalline network, and crystalline mush zones in the solidifying mantle. In this figure, as in the following figures, the planetary radius is shown on the left axis with 0 at the center and 3396 at the surface. The potential temperatures for adiabats are marked at the top of the graph. The dashed line signifies the approximate region of 50% to 60% crystallinity, above which a 3-dimensional crystal network forms. Magma ocean crystallization begins at a potential temperature of approximately 2000 °C and is complete at about 1100 °C. These models assume that the solids remain at the solidus temperature after crystallization.

cool, a partially solid region develops. The presence of solids increases the viscosity of the liquid, and with more than a critical fraction of solid (between about 50% and 60%; Campbell and Forgacz 1990; Marsh 1995; Lejeune and Richet 1995), the viscosity becomes close to that of solid deforming by thermally activated creep. In this layer, crystals form a 3-dimensional network through which liquids are still able to flow.

We assume that, due to diffusion through or flow of interstitial liquid, crystals in this partially solid layer maintain chemical and thermal communication with all the liquid remaining in the magma ocean. Solid phases, except those in the isolated, fully solid material at the bottom of the magma ocean, remain in equilibrium with the liquid in which they are immersed. As solidification and compaction continue at the bottom of this partially solid layer, a fully solid mantle is created. Each successive small increment of this solid layer is, according to this idealization, in chemical equilibrium with the remaining magma ocean above it. Once fully solid, the material in each tiny increment becomes isolated from the magma ocean, with a composition that subsequently remains fixed, thus approximating simple fractional crystallization. If

the rate of crystallization were sufficiently fast, one might envision that each increment of crystallization would retain the initial liquid composition, thus approximating batch crystallization. However, since solidification requires the transfer of heat, one must suppose that for such batch crystallization to occur, heat transfer would have to be much more rapid than chemical transport.

In our model, solid phases are calculated in equilibrium with the liquid, and their components are subtracted from the remaining magma ocean. Crystallization proceeds from the bottom upward in shells of one-half percent of the magma ocean per step. Solid phase compositions are not assumed to diffuse or re-equilibrate, and no retention of interstitial liquids is included in the model. Interstitial liquids would have an important effect on the incompatible trace element content of the cumulate layers and possibly on the viscosity of the layers as well. Further, no late-stage, incompatible-element-enriched fluid (comparable to the KREEP material found on the Moon) is considered in this model.

Though this model does not explicitly treat interstitial liquids, their influence on composition and rheology is important, so a brief discussion of the dynamics of interstitial

liquids is included here. Interstitial liquids are trapped in solidifying liquids when solidification proceeds more quickly than compaction and melt migration. The bottom of the partially solidified zone moves to a shallower depth due to cooling by heat loss at the surface. The upward velocity (V) of this solidification front compared to other transport mechanisms will control the compositional effects of trapped liquids. Buoyant percolation of liquid that is less dense than solid would occur at a pore velocity:

$$u = \frac{K}{\phi\mu} \Delta\rho g \quad (1)$$

where K is permeability, $\Delta\rho$ is the density difference between the crystals and the liquid, μ is the liquid viscosity, and ϕ is the melt fraction. If liquid percolation occurs through tube-like channels along mineral grain edges, then:

$$K \approx \frac{b^2 \phi^3}{200} \quad (2)$$

where b is the grain size (e.g., Wark and Watson 2002). The amount of melt trapped is given by the value of ϕ for which $V \cong u$. Escape of interstitial liquid requires compaction of the solid. This estimate neglects the resistance of deformation of the solid that will further increase the trapped melt fraction (e.g., Shirley 1986). A surface heat flux by radiation through a wet atmosphere (Abe et al. 2000), at a surface temperature equal to the potential temperature of the liquid, would give trapped liquid fractions on the order of 1 to 10% for a grain size of 1 mm and a liquid viscosity of 1 to 10 Pas. If the opacity of the atmosphere were greater, or if a conductive lid formed at the planetary surface, the resulting much lower rates of cooling would give a smaller trapped melt fraction. Even a trapped melt fraction less than 1% may be significant in controlling the incompatible element content of the solidified silicate mantle.

Faster migration of liquid is possible through larger channels; as can be seen by increasing the value of (b) in the above expression for (K). One possibility may be that upwardly percolating liquids form vertical chimneys seen in laboratory experiments and field occurrences (Tait and Jaupart 1992). Localized, channeled liquid flow of this kind can have large effects on residual solid composition. Dissolution of solid mineral phases may control the organization of fluid pathways (Kelemen et al. 1992; Aharonov et al. 1995) and may also have significant implications for mineralogy. Vertical petrological zonation has been shown in ultramafic mantle assemblages with

percolating basaltic magmas by Kelemen (1990). Compaction of the also solids may lead to horizontal segregation veins in terrestrial rocks (Philpotts et al. 1996).

The mantle is assumed to be 2000 km deep, with a pressure of 24 GPa at the core-mantle boundary (a radius of about 1396 km, consistent with the results of Bertka and Fei [1998b], but dependent on the sulfur content of the core, which is unknown). Both Zuber et al. (2000) and Kavner et al. (2001), through different techniques, have arrived at the conclusion that Mars' crust must be no thicker than about 50 km. A 50 km-thick crust represents about 4% of the planet's mass. No low-density crust is calculated during magma ocean crystallization in these models; all minerals are mantle phases.

Assumptions about Petrology

The bulk composition of the martian mantle is assumed to be that of Bertka and Fei (1997) renormalized without Na_2O . At high pressures, the stability of minor phases and the partitioning behavior of minor components into major phases are not known well enough to model their appearance and importance in the martian magma ocean. Therefore, the bulk magma ocean compositions are limited to 5 oxide components, as shown in Table 1. For each bulk composition, the 5 oxides sum to 98% or more and dominate any chemical and physical processes. The bulk compositions of Bertka and Fei (1998a) and Dreibus and Wänke (1985) do not yield significantly different results when used in these models (but, see also Drake and Righter [2002]).

Bertka and Fei (1997) determined high pressure equilibrium phase assemblages experimentally for a likely martian mantle composition, resulting in a mantle with 7 layers of different assemblages. Though the Bertka and Fei (1997) model is the most relevant for our study, it contains both assumptions and complexities unnecessary for the idealized models investigated here. Also, note that the experiments of Bertka and Fei (1997) use the same composition at each pressure, which is certainly unrealistic for a magma ocean in which the liquid composition evolves as crystallization proceeds. We use the simplified phase relations shown in Fig. 2, which are similar to those of Longhi et al. (1992) (see also the detailed calculations of Hofmeister [1983] for a terrestrial magma ocean). Though our mineralogy is significantly simpler than that used by Bertka and Fei (1998a) to model density (they used their 1997 experimental results), our simpler density profile is close to

Table 1. Bulk martian mantle compositions, in weight percent.^a

Source	SiO_2	Al_2O_3	FeO	MgO	CaO	Mg#
Bertka and Fei (1997)	43.90	3.15	18.80	31.66	2.50	75
Dreibus and Wänke (1985)	45.32	3.08	18.27	30.83	2.50	75
Morgan and Anders (1979)	42.06	6.49	15.98	30.17	5.29	77

^aThe composition of Bertka and Fei (1997) is used in this study. All have been renormalized based on 5 oxide components only. Mg# = molar Mg/(Mg + Fe).

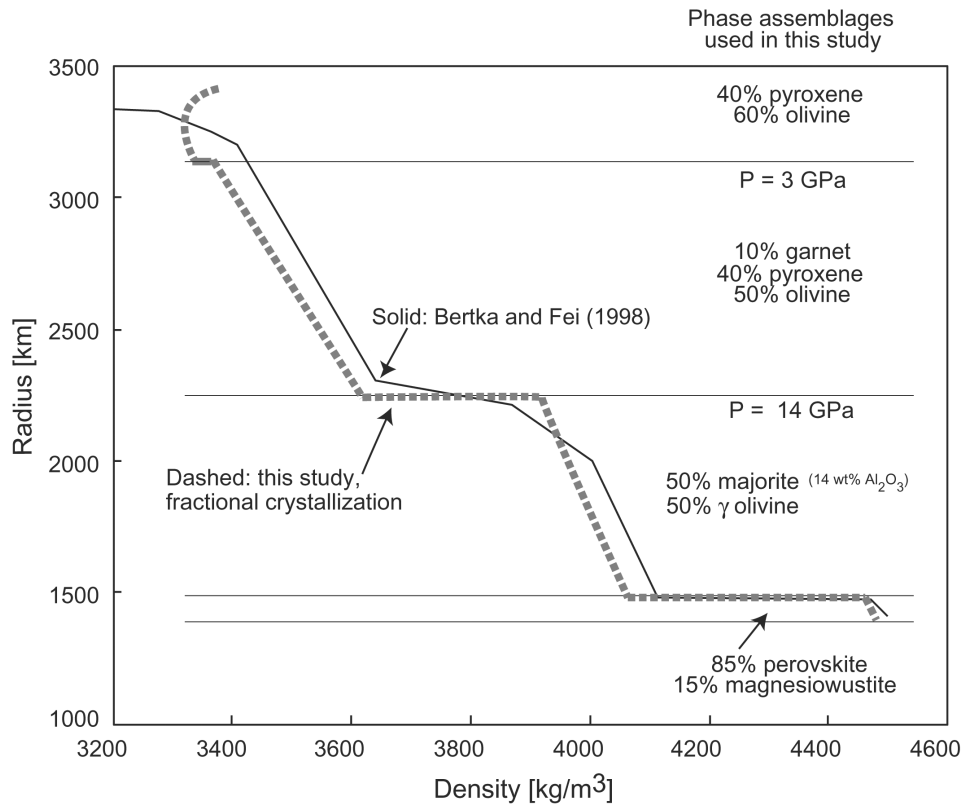


Fig. 2. Comparison of the density profiles produced in this study and those of Bertka and Fei (1998a). Though Bertka and Fei (1998a) used a complex, experimentally-determined phase stratification, our simpler model produces an acceptable match to their prediction. In the remainder of this study, the deepest, perovskite-bearing layer is excluded from calculations.

their prediction. This similarity of results satisfies several questions. It reinforces Bertka and Fei's (1997, 1998a) results by showing their close correlation with theory; it demonstrates that the simple mineralogical model used here is probably sufficiently complex to treat first-order effects; and it shows that complex mineralogical layering is difficult to differentiate from simple layering on the basis of density models and moments of inertia.

Perovskite stability is dependent on the bulk composition, temperature, and pressure in the deep mantle, and these are not well enough constrained for Mars to make an unequivocal prediction (e.g., Longhi et al. 1992; Bertka and Fei 1998a; Halliday et al. 2001). In particular, the sulfur content, and therefore radius, of the martian core is not constrained. Depending on the core composition assumed, the perovskite stability region may lie entirely within the martian core (e.g., Fei et al. 1995). Though we include a perovskite layer in Fig. 2 to compare to the Bertka and Fei (1998a) results, the remainder of the paper adopts a 3-layer model, with no deep perovskite and magnesiowustite layer and neglecting the possible occurrence of other high pressure phases.

In our model, the equilibrium phases for each fractional crystallization increment are calculated using the exchange coefficients in Table 2 and the stoichiometric mineral formulas

Table 2. Exchange coefficients used in calculations.

Phase	$K_{D(\text{Fe-Mg})}^a$	$K_{D(\text{Ca-Al})}$	$K_{D(\text{Si-Mg})}$
Olivine (α olivine)	0.32	—	—
γ -olivine	0.70 ^b	—	—
Clinopyroxene	0.28	—	—
Majorite	0.45 ^{b, c}	0.40 ^c	1.2 ^c
Garnet	0.48 ^b	0.40 ^b	0.8 ^b
Perovskite	0.46 ^c	0.50 ^c	1.1 ^c
Magnesiowustite	2.00 ^d	—	—

^aThe exchange coefficient is defined as follows for $K_{D(\text{Fe-Mg})}$ and analogously for other elements: $K_{D(\text{Fe-Mg})} = (\text{Fe}/\text{Mg})_{\text{mineral}}/(\text{Fe}/\text{Mg})_{\text{liquid}}$, where "liquid" is the silicate melt from which the mineral is crystallizing.

^bCalculated from experiments in Bertka and Fei (1997), assuming an olivine K_D of 0.32.

^cTronnes and Frost (2002).

^dCalculations from experiments in Bertka and Fei (1997) produced K_D s between 1.5 and 3.0.

in Table 3. The exchange coefficient is defined as follows for $K_{D(\text{Fe-Mg})}$, and analogously for other elements: $K_{D(\text{Fe-Mg})} = (\text{Fe}/\text{Mg})_{\text{mineral}}/(\text{Fe}/\text{Mg})_{\text{liquid}}$, where "liquid" is the coexisting silicate melt. The equilibrium pyroxene composition is calculated by further assuming that the molar ratio of molar Ca/(Mg + Fe) in the pyroxene is 0.2. Pinning the Ca/(Mg + Fe) ratio is a gross simplification but is consistent with calculated pyroxenes for the martian mantle from Longhi et al. (1992) and

Table 3. Thermochemical parameters used in calculations.

Phase	Thermal expansivity (/K) $\alpha(T) = \alpha_0 + \alpha_1 T + \alpha_2 T^2$			Bulk modulus (GPa or GPa/°)			Mol. vol. (cm ³ /mol)	Ref. ^a
	α_0	$\alpha_1 (10^5)$	$\alpha_2 (10^9)$	$K_{T, 298}$	$\delta K/\delta P$	$\delta K/\delta T$	V_0	
Olivine (α olivine)								
Forsterite Mg ₂ SiO ₄	3.034	7.422	-0.5381	129	5.37	-0.0224	43.6	c, b
Fayalite Fe ₂ SiO ₄	2.386	11.53	-0.0518	137.9	4.0	-0.0258	46.29	c
γ -olivine								
Mg ₂ SiO ₄	2.497	3.639	-0.6531	183	4.3	-0.0348	39.65	c, d
Fe ₂ SiO ₄	2.697	5.298	-0.5702	197	4.0	-0.0375	42.02	d
Clinopyroxene								
Mg _{0.8} Ca _{0.1} SiO ₃	3.33	0	0	113	4.8	-0.02	66.04	c
Fe _{0.8} Ca _{0.1} SiO ₃	2.98	0	0	119	4.2	-0.02	67.87	c
Majorite								
(Mg, Fe) ₃ Si ₃ O ₁₂	2.874	2.886	-0.5443	160	4.0	-0.022	113.99	a, c, d, e
Garnet								
Grossular Ca ₃ Al ₂ Si ₃ O ₁₂	1.951	8.089	-0.4972	168	6.2	-0.022	125.12	c
Pyrope Mg ₃ Al ₂ Si ₃ O ₁₂	2.311	5.956	-0.4538	179	4.0	-0.022	113.08	c
Almandine Fe ₃ Al ₂ Si ₃ O ₁₂	1.776	12.14	-0.5071	175	4.0	-0.022	115.43	c
Perovskite								
Ca ₃ Al ₂ Si ₃ O ₁₂	3.153	9.421	-0.3271	248	4.44	-0.027	81.96	c, e, f
(Mg, Fe) ₃ Al ₂ Si ₃ O ₁₂	1.982	8.180	-0.4740	261	4.2	0	99.52	e
Mg ₃ Si ₃ O ₁₂	1.982	8.180	-0.4740	261	4.0	-0.028	73.5	a, c, d, e
Fe ₃ Si ₃ O ₁₂	1.982	8.180	-0.4740	287	4.0	-0.028	76.8	a, c, d, e
Magnesiowustite								
MgO	3.768	7.404	-0.7445	160	4.13	-0.0272	11.25	b, c
FeO	3.55	11.0	0	158	4.13	-0.031	12.25	c, g

^aReferences: a = Fei et al. (1990) and references therein; b = Holland and Powell (1998) and references therein; c = Bertka and Fei (1998a) and references therein; d = Fabricznaya (1999) and references therein; e = Akaogi et al. (2002); f = Hama and Suito (2001); g = Zhang and Kostak (2002).

also with the experimentally produced pyroxenes at 6 to 11 GPa from Bertka and Fei (1997) (those at lower pressures contain more CaO). We further simplify the pyroxene compositions by assuming that they contain no aluminum. The majorite equilibrium composition is calculated using the further constraint that the molar Al/Si ratio is 0.4 (from experimental results of Bertka and Fei [1997]). The final mineral formula is (Mg, Fe, Ca)₃Al_{1.2}Si₃O₁₂. Experimental majorite compositions vary from about 4 wt% Al₂O₃ to about 19 wt% Al₂O₃. The majorite compositions in this model have about 14 wt% Al₂O₃. The perovskite equilibrium composition is calculated using the further constraint that the molar Al/Si ratio for the final mineral is 0.09 (from experimental results of Bertka and Fei [1997] and Tronnes and Frost [2002]). The final mineral formula is (Mg, Fe, Ca)₃Al_{0.3}Si₃O₁₂. Experimental perovskite compositions contain about 4 wt% Al₂O₃, as do the compositions in this study (see also Daniel et al. 2001).

Equations of State of Crystallizing Minerals

After calculating the equilibrium phases after each increment of crystallization (one half percent of the mantle), the phases are divided into the components as listed in

Table 1, and their densities are calculated at the appropriate pressure and temperature for their position in the mantle. The pressure for each crystallizing shell is:

$$P = 0.012z \quad (3)$$

with P in GPa and z depth in km. This fit yields a pressure of 24 GPa at 2000 km depth, the bottom of the magma ocean in this model. Knowing the density and mass of the previous crystallized shells allows calculation of the thickness of each shell and, thus, the depth of each subsequent shell. The temperature for each shell is calculated from the following fit to Longhi et al.'s (1992) solidus for the martian mantle, shown in Fig. 1:

$$T_{1396\text{km} > r > 3396\text{km}} = (-1.96 \times 10^{-10})r^4 + (1.69 \times 10^6)r^3 - (0.0053)r^2 + (6.8437)r - 930 \quad (4)$$

where T is temperature in Celsius, and r is martian radius in km from the center of the planet. Once the temperature is known, the molar volume of the phase at 1 atm and the model temperature is calculated separately from the parameters given in Table 2 as:

$$V_0 = V_0^{298} \exp\left[\int (\alpha_0 + \alpha_1 T + \alpha_2 T^2) dT\right] \quad (5)$$

where T is temperature in degrees Kelvin. The pressure effect on density is then calculated separately for each phase using the parameters in Table 2 and the following Burch-Murnaghan equation of state:

$$P = \left(\frac{3}{2}\right) K_T \left[\left(\frac{V_0}{V}\right)^{\frac{7}{3}} - \left(\frac{V_0}{V}\right)^{\frac{5}{3}} \right] \left\{ 1 - \left(\frac{3}{4}\right) (4 - K'_T) \left[\left(\frac{V_0}{V}\right)^{\frac{2}{3}} - 1 \right] \right\} \quad (6)$$

where we solved iteratively for the molar volume, V , at pressure and temperature by adjusting the pressure, P , from the Burch-Murnaghan equation until it matched the model pressure to within an accuracy of 0.1 GPa. K'_T is the pressure derivative of K_T , the isothermal bulk modulus, at constant temperature:

$$K'_T = \left(\frac{\delta K_T}{\delta P} \right)_T \quad (7)$$

given in Table 2 for each phase. The K_T appropriate for the temperature within each shell is:

$$K_T = K_{T, 298} + \left(\frac{\delta K_T}{\delta T} \right)_P (T - 298) \quad (8)$$

where T is temperature in Kelvin. The temperature derivative of K_T and $K_{T, 298}$ are both listed in Table 3 for each phase. Calculated reference densities for the phases in these models are shown in Table 4. Having calculated the density of each phase, the bulk density of the phase assemblage is calculated from the a priori assumption of the phase fractions, and the thickness of the layer can then be calculated.

Relative Densities of Solids and Liquids: Effect of Fractional Solidification

As a magma ocean crystallizes, crystals are expected to form at the base of the magma ocean, where the adiabat intersects the solidus, and in cold downwellings generated by heat loss at the planetary surface. In our idealization, the development of each successive increment of solidified mantle requires that some crystals settle rather than staying suspended and re-equilibrating with the liquid.

Our first model, which we term the simple fractional crystallization model, considers that the next solid increment consists of all minerals that would be in equilibrium at the appropriate solidus temperature and pressure. A second model, which we term the garnet segregation model, accounts for fractionations that may arise from density differences between solids and the liquid in which they are immersed. As previous investigators have discussed (e.g., Stolper et al. 1981; Agee and Walker 1988; Franck 1992; Morse 1993; Ohtani et al. 1995), olivine and pyroxene sink with respect to magma ocean liquids at shallow depths, but at pressures greater than about 7.5 to 9 GPa, depending on composition,

Table 4. Calculated reference densities for the phases in these models.^a

Phase	Density at 1 atm and 1°C (kg/m ³)
Olivine (α olivine)	
Forsterite Mg ₂ SiO ₄	3227
Fayalite Fe ₂ SiO ₄	4402
γ -olivine	
Mg ₂ SiO ₄	3549
Fe ₂ SiO ₄	4850
Clinopyroxene	
Mg _{0.8} Ca _{0.1} SiO ₃	3240
Fe _{0.8} Ca _{0.1} SiO ₃	3900
Majorite	
Mg ₃ Si ₃ O ₁₂	3523
Fe ₃ Si ₃ O ₁₂	4630
Garnet	
Grossular Ca ₃ Al ₂ Si ₃ O ₁₂	3600
Pyrope Mg ₃ Al ₂ Si ₃ O ₁₂	3565
Almandine Fe ₃ Al ₂ Si ₃ O ₁₂	4312
Perovskite	
Ca ₃ Al ₂ Si ₃ O ₁₂	5669
Mg ₃ Al ₂ Si ₃ O ₁₂	4051
Fe ₃ Al ₂ Si ₃ O ₁₂	5002
Mg ₃ Si ₃ O ₁₂	5464
Fe ₃ Si ₃ O ₁₂	6872
Magnesiowustite	
MgO	3583
FeO	5865

^aIn the models, density is calculated for the specific composition, temperature, and pressure needed, using the parameters in Table 3.

olivine and pyroxene become positively buoyant with respect to the liquid and float. In the model presented here, the crossover pressure below which olivine is positively buoyant is calculated to be 7.5 GPa, within the range of estimates of other workers (see Fig. 3).

Mineral physics calculations indicate that, while olivine and pyroxene are buoyant in this pressure range, garnet is more dense than coexisting liquid at pressures greater than ≈ 7.5 GPa (≈ 600 km depth in Mars), as shown in Fig. 3. A crystallizing magma ocean may allow garnet to sink from the low velocity flow near the bottom boundary, while olivine and pyroxene either rise to form a layer at their depth of neutral buoyancy, or remain suspended in vigorous convection away from solid boundaries. This depth of neutral buoyancy is near the center of the convecting layer where vertical velocities are the highest. For the vertical convective velocities of the magnitude expected in a vigorously convecting magma ocean (Solomatov [2000] estimates velocities can be in the tens of meters per second), olivine and pyroxene are likely to remain suspended rather than segregate into a layer at their depth of neutral buoyancy.

In the garnet segregation model, at pressures less than

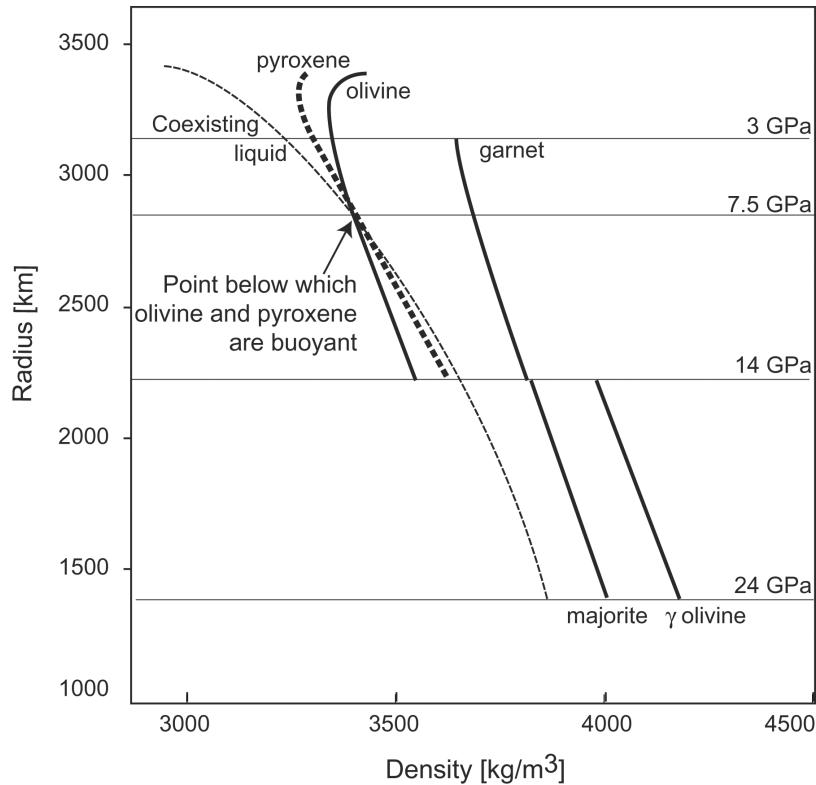


Fig. 3. Densities of individual mineral phases and the residual liquid from a simple fractional crystallization model. Both olivine and pyroxene are positively buoyant over the first half of their crystallization interval, leading to the likelihood of forming a dense, monomineralic garnet layer as heavy garnet sinks from the lowest, laminar flow portion of convective flow and pyroxene and olivine float.

14 GPa, garnet sinks while olivine and pyroxene remain suspended in a well-mixed magma ocean liquid. Garnet is, therefore, fractionally crystallized from the magma ocean liquid and sequestered. At a pressure of about 11.4 GPa (~950 km depth), aluminum is sufficiently exhausted from the remaining magma ocean liquid that garnet no longer crystallizes. Though the possibility of complex liquid and solid layering exists in this scenario, we consider only the simplest case, with a well-mixed layer during garnet fractionation followed by a well-mixed layer during olivine and pyroxene fractionation. Olivine and pyroxene crystallize in equilibrium with the remaining liquid and complete the cumulate stratigraphy. In this model, the olivine and pyroxene crystallization after garnet exhaustion is treated as simple fractional crystallization in a well-mixed liquid rather than considering the possibility of a septum at the depth of neutral buoyancy.

Whether crystals remain suspended or settle out is fundamental to understanding the chemical evolution of a magma ocean. Mass conservation requires that the average vertical velocity of convective motions across any horizontal plane in the magma ocean vanish, so both upward and downward fluid motions must occur. The settling of dense crystals results in persistent sinking relative to convecting liquid, so crystals must settle out even if the settling velocities are small compared to convective motions (Marsh 1988;

Martin and Nokes 1989). The ability of crystals to accumulate at the bottom depends on a competition between settling and entrainment (Martin and Nokes 1989; Tonks and Melosh 1990; Solomatov and Stevenson 1993a, b; Solomatov 2000). Adjacent to a horizontal boundary, vertical velocities are small. However, convective motions can move particles horizontally along the boundary toward regions of convergence beneath buoyant upwellings, where viscous stresses can lift the particles. Laboratory experiments on a fluid layer heated from below suggest that particles smaller than diameter D can be entrained in this way (Solomatov et al. 1993), where:

$$D \approx \frac{10}{\Delta\rho g} \left(\frac{\eta\alpha g F}{c_p} \right)^{1/2} \quad (9)$$

Here, $\Delta\rho$ is the density difference between the particles and the liquid, g is the acceleration of gravity, η is the fluid viscosity, α is the coefficient of thermal expansion, c_p is the specific heat, and F is the heat flux transported by convective motions. Thus, higher viscosity and higher heat flux result in larger particles that can be entrained. Heat flux F can range from 10^{-4} to 1 W/m², depending on the existence of an atmosphere (Abe and Matsui 1985; Solomatov et al. 1993; Abe 1997). For liquid of picritic composition at high pressure, $\eta = 0.1$ Pas (Bottinga and Weil 1972; Shaw 1972).

Using values of 200 kg for $\Delta\rho$, 3.7 m/s² for g (although g will be lower at smaller radii in the planet), 0.1 Pas for η , 3E-5 /° for α , 1 W/m² for F , and 1256.1 J/°kg for c_p , Equation 7 indicates that particles larger than 10⁻² mm will not be entrained. The value of 0.1 Pas is consistent with values from Solomatov (2000) but higher than values from Rubie et al. (2003); lower viscosities would allow smaller mineral grains to settle. If the effect of crystallinity is considered, however, effective viscosity may be much larger. Another consideration is how fast crystals grow once they are nucleated. Smaller entrained crystals could continue to grow until reaching a size at which they will settle out.

These results apply to heating from below. In a magma ocean cooling by heat loss at the planetary surface, cold downwellings are expected to provide a significant fraction of the convective heat flux. Experiments indicate that cold downwelling plumes do not entrain particles from the lower boundary. Therefore, the heat flux in Equation 7 should only be that derived from the heat of crystallization and carried by the hot plumes, perhaps a small fraction of the total convective heat flux.

Mechanisms for Overturn

Three main factors control the creation of cumulate density profiles with compositionally denser mantle overlying less dense mantle, thus, prone to overturn: 1) the residual magma ocean liquid evolves, producing denser minerals as crystallization proceeds; 2) the assemblage of stable minerals changes, producing density changes inherent to the crystal structures in addition to those caused by the liquid composition; and 3) the mineral phases have differing compressibilities, and, therefore, their densities change differently in response to pressure.

To determine the stability of the cumulates, densities must be compared at a common reference pressure. To consider only the effect of composition, densities must also be compared at a reference temperature. Because cumulates in our models remain at their solidus temperature, we also include the effect of thermal expansion on the density distribution. Comparison is made at a reference pressure because of the mechanism for overturn: cooler, denser material falling from shallow levels displaces material originally in the deep mantle to higher levels. The deep material displaced upward will then facilitate or hinder overturn depending on its density relative to the material at the level to which it has risen. The relative densities at the same pressure, not the densities of the materials at their original pressures, need to be compared to assess stability relative to overturn.

Lower mantle densities require a further adjustment to predict the tendency of overturn. The lowest mineralogical layer, containing 50% majorite + 50% γ -olivine, is about 7% more dense than the upper mantle average while at its solidus

temperature. If, however, cool drips from the upper mantle fall into the lower mantle, majorite + γ -olivine displaced upward will revert to a less dense garnet + pyroxene + olivine mineralogy. To compare stability, we recalculate the lower mantle composition as a garnet + pyroxene + olivine mineralogy. The 50% majorite + 50% γ -olivine layer, converted into stoichiometrically equivalent upper mantle phases, results in a phase assemblage of 20% garnet + 30% pyroxene + 50% olivine. Temperature changes due to the heat of reaction during this adiabatic decompression may also affect the relative density but are small compared to the density change due to changing the assemblage of minerals. The density profile used to assess stability, then, consists of the upper 2 cumulate layers calculated at their solidus temperatures and 1 atm pressure and the lowest, majorite + γ -olivine layer recalculated as garnet + pyroxene + olivine.

If the density profile thus obtained is found to be unstable, an idealized overturn is calculated by sorting the original shells of material by density into a new, stable stratification in which density decreases monotonically upward. The volume of each shell is conserved, and temperatures are adjusted for adiabatic rise or fall. Since rising material cools and descending material heats up, adjusting for adiabatic rise or fall reduces the temperature range in the overturned mantle. This idealized overturn model assumes that freezing is fast compared to the overturn time of any already solidified portion and that cold downwellings from the top of the solidified layer completely displace deeper, lower-density layers so that all layers are perfectly reshuffled.

The Rayleigh-Taylor instability and overturn of an unstably stratified layer of viscous fluid of thickness (d) and viscosity (η) with stress-free top and bottom boundaries is:

$$t_{\text{overturn}} = \frac{4\pi^2\eta}{\gamma g d^2} \quad (10)$$

where γ is the compositional density gradient and g is gravity (Hess and Parmentier 1995). As the thickness of the solidified layer (d) increases, its overturn time decreases. Gravity also increases with height above the core-mantle boundary, further decreasing overturn time as the solidified layer thickens. At the beginning of solidification at the core-mantle boundary, when d is small and g is about 3.1 m/s², the overturn time of a 100 km-thick layer with $\gamma = 5 \times 10^{-5}$ kg/m³/m and $\eta = 10^{20}$ Pas is about 100 Myr. The value of viscosity is taken to be comparable to values near the bottom of the Earth's upper mantle, in the range 10²⁰–10²¹ Pas. Near the end of solidification, when d is 20 times thicker, the overturn time is only a fraction of a million years. Overturn, therefore, involves a competition between the rate of thickening and the Rayleigh-Taylor time scale of the solidified layer. The time required to crystallize a magma ocean depends strongly on the rate of heat transfer at the planetary surface. The results of

Franck (1992) imply that a magma ocean the depth of the martian mantle would crystallize in less than 100 Myr; perhaps orders of magnitude less, depending on surface temperature and patterns of convection. Abe's (1997) results indicate that this magma ocean would crystallize in about 30 Myr. Both Davies (1990) and Solomatov (2000) suggest that the deepest magma ocean may crystallize in on the order of 10^3 yr, but final crystallization of the shallow ocean may take as long as 10^8 yr.

Overtun rates do not, therefore, become significantly less than thickening rates until near the end of magma ocean solidification, and so, even for conservative magma ocean crystallization times, the ocean can be expected to crystallize before overturn can occur. Other effects may shorten overturn time; for example, circulating interstitial liquids could significantly reduce the effective viscosity of the solid ocean, speeding overturn. Should overturn begin before crystallization is complete, however, little difference in outcome is expected for the models presented here.

Phase Changes and the Stability of Overturn

Since the temperature distribution after rapid solidification lies along the solidus (see Fig. 1), overturn requires that cool material at shallow depth be displaced downward and hotter material at depth be displaced upward. The relative depth or pressure at which phase transitions occur in these ascending and descending currents can either hinder or promote convective instability (Schubert and Turcotte 1971; Schubert et al. 1975) depending on the Clapeyron slope of the phase transition. If dP/dT slope of the phase boundary between two mineral assemblages is positive, the denser lower pressure phase forms at a lower pressure or shallower depth in cold material than in pre-existing hotter material through which it is sinking, thus promoting instability and overturn. In this case, the transformation to the denser phase is exothermic. If, conversely, the Clapeyron slope is negative, the endothermic reaction to the denser assemblage occurs at higher pressure or greater depth in sinking lower temperature material so that cool sinking material has to be pushed more deeply than existing warm material to undergo the phase change. The requirement of pushing less dense material into deeper, denser material is a hindrance to the fall of cool material.

The Clapeyron slope can be calculated as:

$$\frac{dP}{dT} = \frac{\Delta S}{\Delta V} \quad (11)$$

where ΔS and ΔV are the entropy and volume change of the reaction, respectively, and T and P are the temperature and pressure at the phase boundary. The key phase boundaries are, therefore, the olivine to γ -olivine boundary and the garnet + pyroxene to majorite boundary. The olivine to γ -olivine reaction is exothermic, at about +3 MPa/K (while the γ -olivine

to perovskite transition is endothermic, at about -3 MPa/K) (Bina and Helffrich 1994).

Presnall and Gasparik (1990) studied the high pressure transition of pyroxene in the $MgSiO_3$ system, and found the transition at about 16 GPa in this Fe-free system. Above about 1600°C, clinoenstatite transforms to majorite across a slightly endothermic boundary with a slope between 0 and -1 MPa/K. Below 1600°C, clinoenstatite transforms to wadsleyite + stishovite across an exothermic phase boundary with a Clapeyron slope of about +1.5 MPa/K. Litasov and Ohtani (2002) carried out experiments in the CMAS-pyrolite system and also found that the clinopyroxene transition has a negative slope. In their results, garnet + wadsleyite + clinopyroxene transforms to majorite + wadsleyite across a phase boundary with a slope of about -1.5 MPa/K.

The olivine to γ -olivine reaction boundary for Bertka and Fei's (1997) martian mantle composition begins at about 12 GPa and is complete at about 15.5 GPa, after passing through small intermediate olivine + γ -olivine and γ -olivine + wadsleyite intervals. For the same composition, the pyroxene to majorite transition, identified by the change from 3 to ~ 3.7 Si cations and 2 to ~ 0.6 Al cations per 12 oxygens, begins at about 13 GPa and is concluded by about 16 GPa (Bertka and Fei 1997). Based on this study, 2 transitions can be modelled reasonably as occurring at the same pressure, which we do in this study. Though neither Litasov and Ohtani (2002) nor Presnall and Gasparik (1990) used a composition close to the martian mantle composition of Bertka and Fei (1997), and their phase transitions differ from the garnet + olivine + pyroxene = majorite + γ -olivine transition used in this model, their results do indicate that the garnet + pyroxene = majorite transition is slightly endothermic. Because the olivine transition and the pyroxene transition are modeled to occur at the same pressure in this study, the Clapeyron driving force can be estimated to be exothermic on the whole, and support overturn, because olivine is both volumetrically larger in this model, and its Clapeyron transition has a larger absolute value.

RESULTS

The simple fractional crystallization model using the Bertka and Fei (1998a) martian mantle composition results in the density profile shown in Fig. 2. Densities at a single reference pressure (1 atm), as appropriate for assessing stability, are shown in Fig. 4. Two profiles are shown, one at a common temperature of 1°C (solid line) and the other (dashed) accounting for thermal expansion due to differing solidification temperatures with depth in the mantle. This demonstrates the importance of the cooler upper mantle temperatures in creating a more dense upper mantle that is unstable and prone to overturn. The lower mantle composition recalculated as 20% garnet + 30% pyroxene + 50% olivine, for comparison with the mid-mantle densities, is

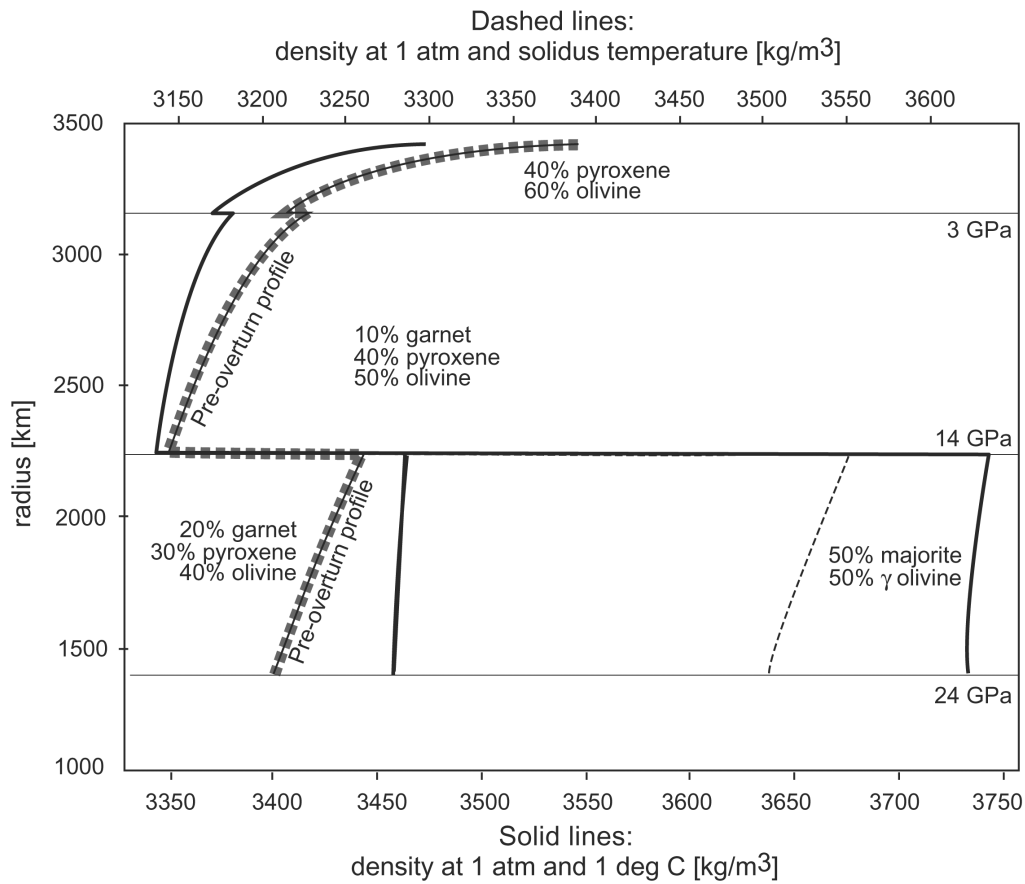


Fig. 4. Density profiles resulting from simple fractional crystallization of the martian magma ocean. Solid lines: all densities calculated at 1 atm pressure and 1°C; dashed lines: densities recalculated at their solidus temperatures and 1 atm. The lower mantle mineralogy recalculated as stoichiometrically correct 20% garnet + 30% pyroxene + 50% olivine is shown to allow direct comparison with the density of the material just above it. The density profile for determination of overturn is labeled “pre-overturn profile.”

also plotted on Fig. 4. The density profile appropriate for assessing stability to overturn is the dashed line labeled “pre-overturn profile.”

The varying compositions of the crystallizing minerals lead to strong compositional stratification in the solidified magma ocean, shown as the variation of major element oxides with depth in Fig. 5. The deepest majorite + γ -olivine layer accumulates aluminum in the lowest layer of the mantle. Iron is increasingly enriched in the cumulates as crystallization proceeds, leading to the higher density of shallower cumulates. The lower K_D s (see Table 2) of olivine and pyroxene are particularly efficient at iron and magnesium fractionation, leading to the increasingly steep MgO and FeO curves in Fig. 5a.

The pre-overturn profile in Fig. 4 shows the most dense cumulates at the surface but the lowest density cumulates at a radius of about 2200 km, marking the bottom of the garnet + pyroxene + olivine layer. Therefore, as the mantle overturns, the most shallow portions will sink to the bottom, and the deepest garnet-bearing layer will rise to the top. The center of the overturned mantle will be a highly heterogeneous mix of the original majorite + γ -olivine layer and the upper layers.

When combined with the compositional information from Fig. 5, we can see that the overturned mantle from the simple fractional crystallization model will have its highest Al_2O_3 values in the center of the overturned mantle, its highest FeO at the bottom, and the highest MgO at the top. This is shown in Fig. 5b.

The heterogeneous post-overturn mid-mantle, seen in Fig. 5 and later in Figs. 8 and 9, is the result of the assumption that the mantle can completely reshuffle on every scale into a monotonically decreasing density profile. The scale of heterogeneity is not a function of step size in the model; step size is small enough that smaller step sizes do not change the model predictions. In reality, the ability of the mantle to reshuffle in response to density will depend on viscosity, and a non-monotonic, laterally heterogeneous mantle, with larger-scale vertical heterogeneities, may result.

For the garnet segregation model, the resulting density profile is presented in Fig. 6. The lowest mantle layer is identical to that in the simple fractional crystallization model. Above 14 GPa, the monomineralic garnet layer is almost as dense as the majorite + γ -olivine layer that underlies it and is far more dense than that layer recalculated as garnet-

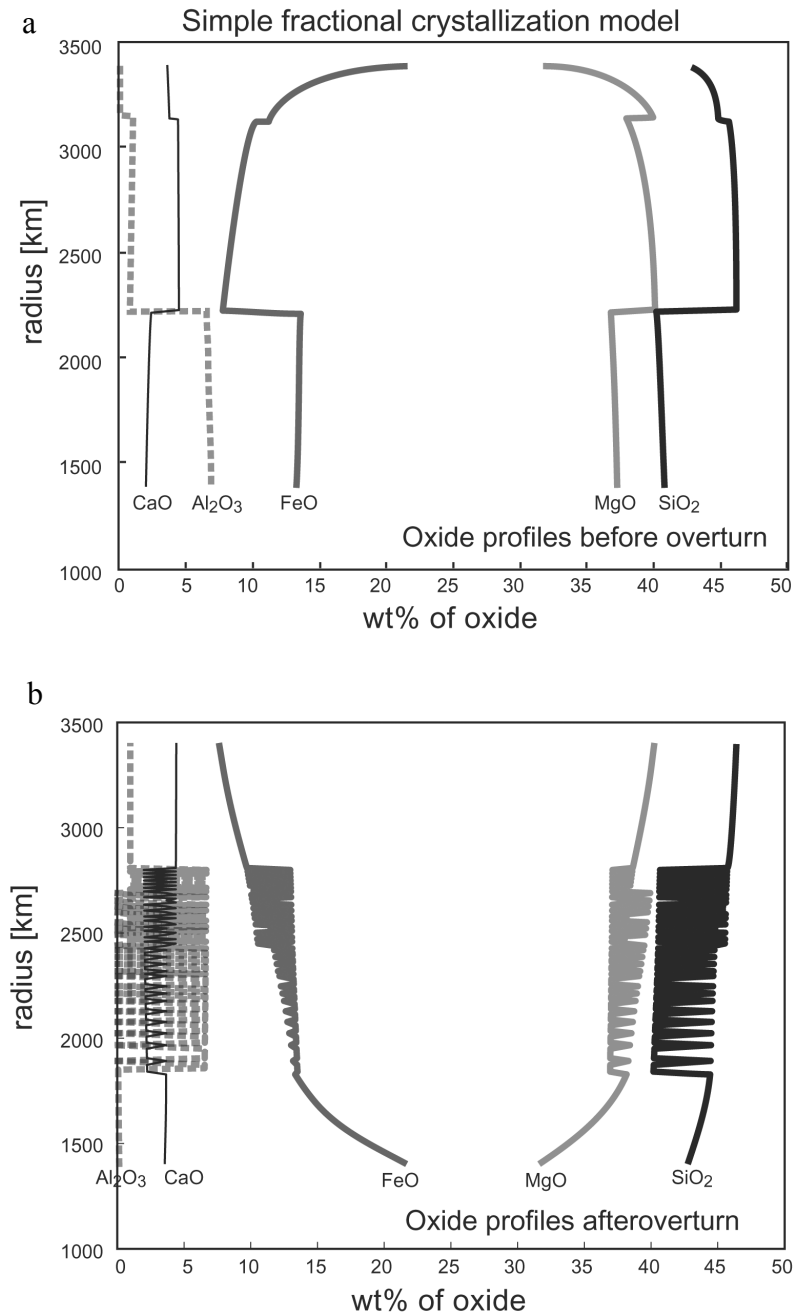


Fig. 5. Compositional stratification resulting from simple fractional crystallization of the magma ocean as shown in Fig. 2. In (a), before overturn, the deepest majorite + γ -olivine sequesters aluminum in the lower mantle. In (b), after overturn, the highest alumina and lowest silica are distributed heterogeneously in the mid-mantle. The lowest mantle has no alumina, and the most shallow mantle has the lowest FeO, but otherwise the most shallow and most deep mantles are compositionally similar. The greatest heterogeneity is produced in the mid-mantle.

pyroxene-olivine mineralogy for the analysis of stability, as discussed earlier. The pre-overturn profile for the garnet segregation model, therefore, has a very dense, highly aluminous layer between 2220 and 2440 that, during overturn, falls into the deepest layers of the mantle.

Idealizing overturn as described above, the pre- and post-overturn density profiles for the 2 models are shown in Fig. 7. The larger range of densities in the garnet segregation model

is evident when compared to the simple fractional crystallization model. The garnet segregation model, thus, has a higher driving force for overturn; the most dense layer in this model is at a higher temperature and, therefore, lower viscosity than the most dense layer in the simple fractional crystallization model, allowing easier overturn. The final density profile has a far more stable, dense lowest mantle than that in the simple fractional crystallization model. The resulting compositional

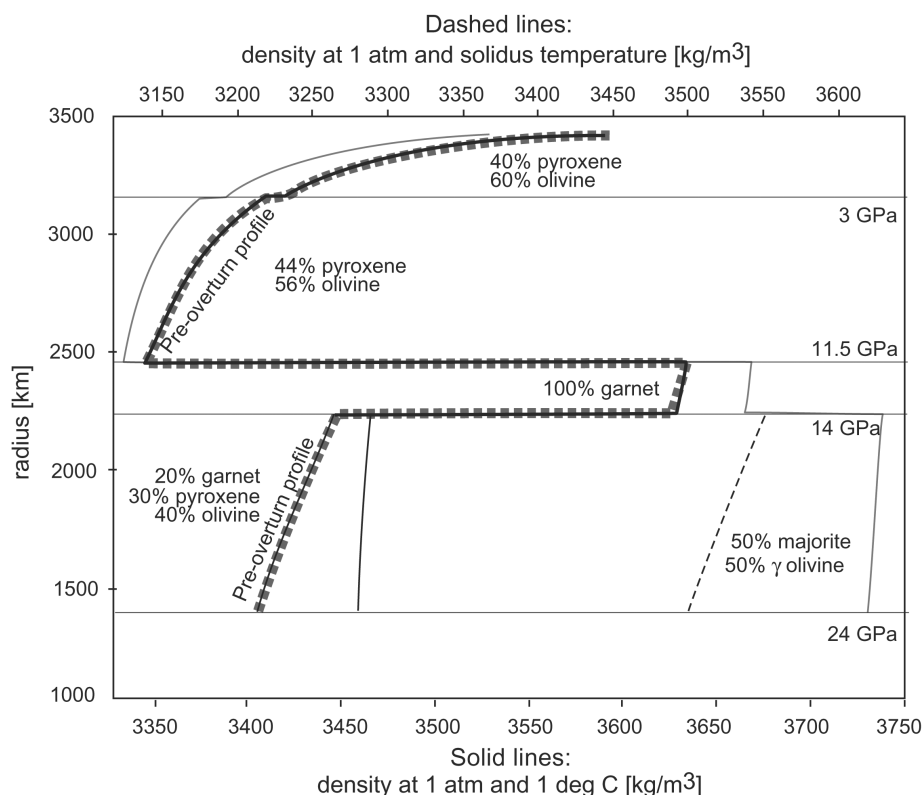


Fig. 6. Density profiles resulting from the garnet segregation model. In this model, when garnet begins crystallizing at 14 GPa, it sinks and forms a monomineralic layer while olivine and pyroxene float, until alumina is exhausted and the remaining cumulates are formed from olivine + pyroxene. Solid lines: all densities calculated at 1 atm pressure and 1°C; dashed lines: densities recalculated at their solidus temperatures. The lower mantle mineralogy recalculated as stoichiometrically correct 20% garnet + 30% pyroxene + 50% olivine is shown to allow direct comparison with the density of the material just above it. The final density profile for determination of overturn is the dashed line labeled “pre-overturn profile.”

profiles after overturn of the garnet segregation model are shown in Fig. 8. The lowest layers of the mantle are the highest in Al_2O_3 and the lowest in FeO, leaving the rest of the mantle as a possible low Al_2O_3 , high FeO source material for SNC meteorites and other magmatic activity on Mars.

In Fig. 7, the densities in the overturned stratification are those of the pre-overturn materials; that is, no re-equilibration to the mineral modes appropriate to the new pressures occurs. For example, the cool, relatively iron-rich olivine that falls into the deep mantle will recrystallize into γ -olivine, and so on for the other reorganized phases. However, recrystallization to denser phases will not change the final compositional stratigraphy.

DISCUSSION

Melting During Overturn

During overturn, when hot material rises from depth, it can cross its solidus through decompression and undergo partial melting. The simple fractional crystallization and garnet segregation models produce complex temperature profiles. Because layers are reordered from most dense to

least dense, the mid-mantle becomes a heterogeneous mix of deep and shallow material, leading to noncontinuous profiles in both temperature and composition, as shown in Figs. 5 and 8. In Fig. 9, the heterogeneous mid-mantle temperature is shown as an average in bold. In regions where temperatures are above the solidus, the temperature profiles shown represent the thermal energy available to produce melt not the temperatures of the remaining solids after melting. The solidus and liquidus shown, taken from Longhi et al. (1992), are not calculated for the specific cumulate compositions that end up at the top of the overturned cumulates. The shallowest cumulates after overturn came from 1000 to 1200 km depth in the magma ocean and would have a higher Mg# than the bulk silicate Mars and, therefore, might have a higher melting temperature than shown. The calculation of melting after overturn given here is only approximate but is sufficient to make a broad statement about crustal formation.

Overturn in both the simple fractional crystallization (Fig. 9a) and the garnet segregation (Fig. 9b) models produces partially molten regions extending from the top of the mantle to a depth of about 900 km. When heats of fusion are taken into consideration, the melt produced is sufficient to create 200 km of crust over the planet’s surface, while crustal depth

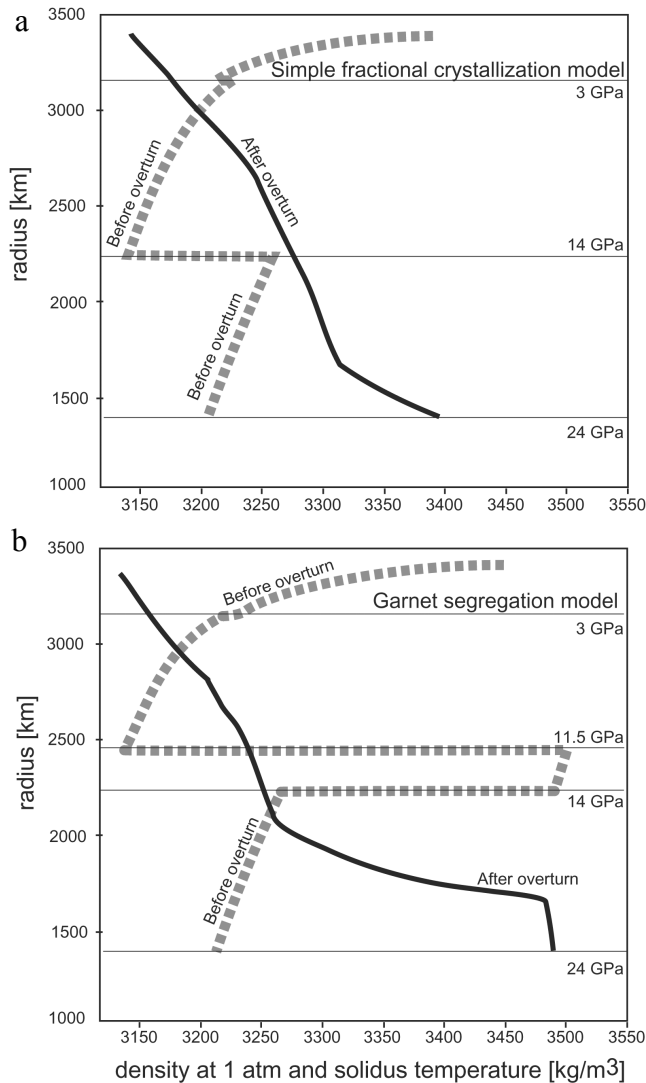


Fig. 7. Comparison of pre- and post-overturn density profiles. In (a), the simple fractional crystallization model is shown. In (b), the garnet segregation model is shown. The greater impetus for overturn and the greater stability of the final profile of the garnet segregation model are evident.

estimates for modern Mars are only about 50 km (Zuber et al. 2000; Kavner et al. 2001). Only about 30% of the total melt produced by overturn in the garnet segregation model is required to create 50 km of crust over the martian surface. However, for several important reasons, the amount of crust predicted in our simple models may be an extreme upper limit on the amount of crust actually produced. First, segregation of this melt from the melting cumulates may be incomplete. Also, decompression melting during overturn may not be completely adiabatic, leading to smaller amounts of melting. Finally, the presence of a cool high viscosity lid at the top of the mantle could also limit the height to which decompressing mantle can rise. A lid thickness of 150 km would reduce the amount of crust produced to about 50 km, even in the absence

of other processes that reduce the melt volume. Conductive cooling for a period of about 100 Myr would be sufficient to produce a lid of this thickness.

Thermal Convection from the Upper Boundary After Overturn?

Since the early planet is envisioned as hot and active, this state has usually been assumed to lead to vigorous convection (e.g., Schubert and Spohn 1990). However, stable compositional stratification after overturn would inhibit thermally driven convection due to cooling at the surface or heating at the core mantle boundary.

At the upper boundary of the overturned cumulate stratigraphy, a similar phenomenon can be caused by cool drips falling from the bottom of a rheologically defined stagnant lid. Though the cumulates are now compositionally stably stratified, drips from the upper boundary can be caused over time by density differences from thermal contraction. The analysis of Zaranek and Parmentier (Forthcoming) shows that, for low background viscosity (10^{17} Pas), convection from the upper boundary can start as early as 10 Myr after overturn for an activation energy of 250 kJ/mol (Fig. 10). With a higher background viscosity of 10^{18} Pas, convection might begin at about 100 Myr after overturn. If the background viscosity were as high as 10^{19} Pas, or if the activation energy were high, convective instability at the upper boundary would be completely suppressed. If convective instability at the upper boundary does occur, convective downwellings will penetrate only to a depth of about 500 km into the underlying, compositionally stratified mantle.

Cool convective downwellings result in a broad upwelling counterflow in which adiabatic decompression melting may occur. In the garnet segregation model, this adiabatic melting would produce melts from a source that is very low in Al_2O_3 and relatively high in FeO, making it a reasonable source for low Al_2O_3 , high FeO shergottite magmas. Blichert-Toft et al. (1999) further suggest, based on Hf and Nd, that garnet was present at some point in the evolution of their mantle source, even though experimental work shows that garnet is not on the liquidus of shergottite primary melts. This is consistent with our garnet segregation model, in which crystallizing garnet lends a recognizable signature to the REE profile of the remaining mantle materials, but the garnet itself has sunk and is not present during the later melting events that produce the shergottites. This upper boundary convection, if initiated, is a good candidate for a process that could continue throughout martian evolution, producing the young igneous rocks seen in the SNC meteorite collection.

Convective stabilization by the compositional stratification may prevent mixing in the interior, thus potentially accounting for the isotopic heterogeneity thought to exist in Mars. ^{182}Hf - ^{142}Nd and ^{146}Sm - ^{142}Nd both indicate

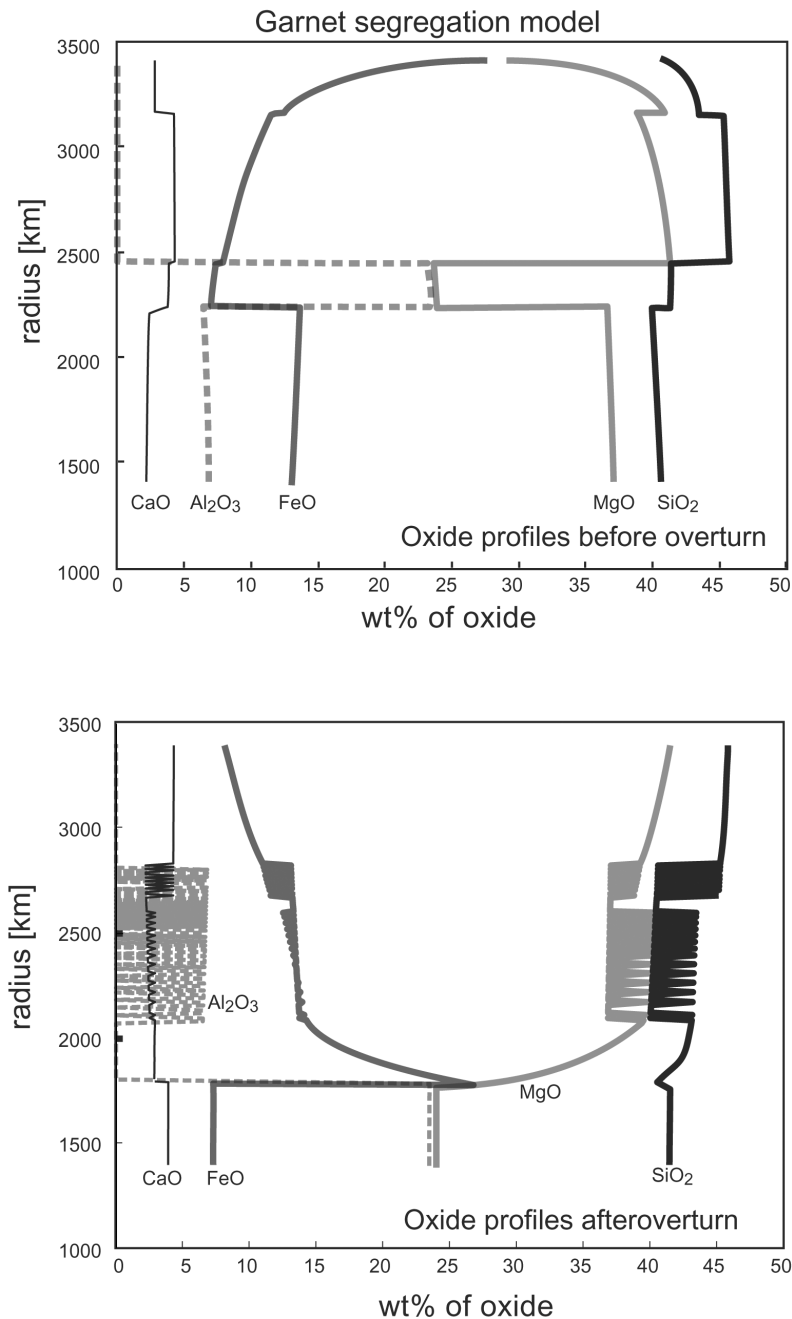


Fig. 8. Compositional stratification resulting from overturn of the garnet segregation model for magma ocean crystallization. After overturn, the highest alumina and lowest iron are sequestered in the lowest mantle. The greatest heterogeneity is produced in the mid-mantle, but the depth of this heterogeneous layer is less than that of the simple fractional crystallization model (see Fig. 5).

early isolation and little subsequent mixing among mantle reservoirs (e.g., Brandon et al. 2000). In the absence of mixing, the chemical stratification of the planet could even persist to the present day. In fact, the density distribution resulting from the garnet segregation model is consistent with the measured moment of inertia of Mars. Folkner et al. (1997) reports the moment-of-inertia factor for Mars to be 0.3662 ± 0.0017 , based on physical data from the Mars Pathfinder. Bertka and Fei's (1998a, b) density profile (shown in Fig. 2)

results in a moment-of-inertia factor of 0.368 for a 200 km-deep mantle over a core with 14% sulfur and no crust (the analogous condition to our model).

After overturn, the moment-of-inertia factor for the simple fractional crystallization model is 0.370, slightly higher than the best current estimates for Mars. The moment-of-inertia factor for the overturned garnet segregation model is 0.366, in excellent agreement with Folkner et al.'s (1997) best estimate. Before overturn, the moment-of-inertia factors of the

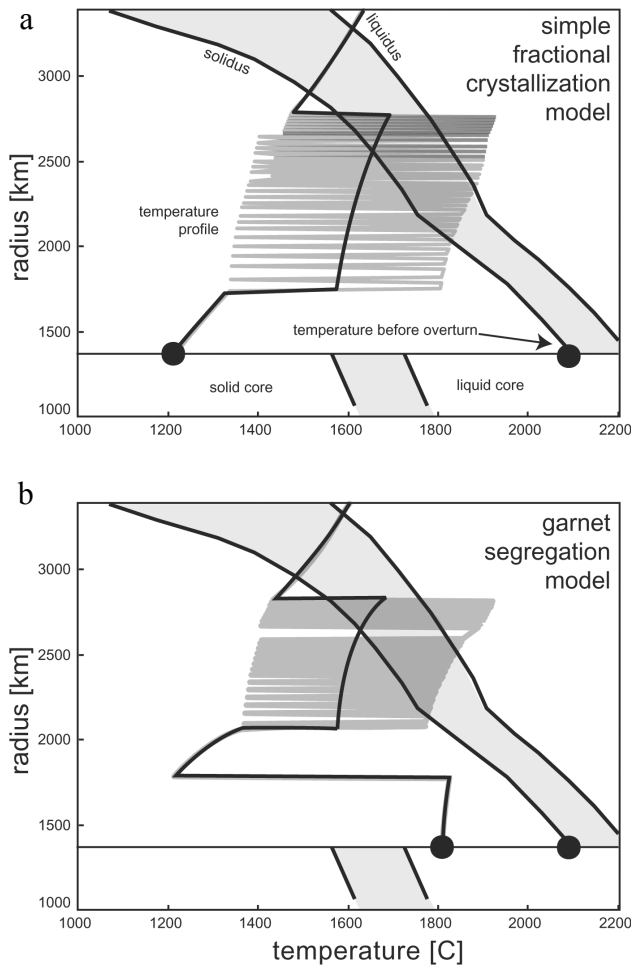


Fig. 9. Remelting of the martian cumulate pile as a result of overturn. When the hot material rises from depth, it can cross the solidus through depressurization and produce melt. In (a), the overturn of the simple fractional crystallization model produces a partial melt to a depth of about 900 km. In (a) and in (b), overturn results in a mid-mantle heterogeneous in composition and temperature, shown in the grey line. The approximate average temperature is shown in black. In (b), the overturn of the garnet segregation model also produces a partially melted mantle to a depth of about 800 km.

two models are 0.364 and 0.363, respectively. Though further modification of the overturned density profile is possible, for example, by mixing and cooling due to solid-state thermal convection from the upper boundary, the existence of a deep, dense, stable layer is, in fact, not inconsistent with observations of Mars today. This deep layer is an effective way to sequester alumina from the SNC meteorite source and may reduce the necessity of suggesting that the bulk martian silicate mantle is depleted in Al_2O_3 and enriched in FeO relative to bulk silicate Earth or chondritic meteorites.

Implications for the Magnetic Field

The processes described in this paper provide 2 possible mechanisms for creating high core-mantle heat flow, and an

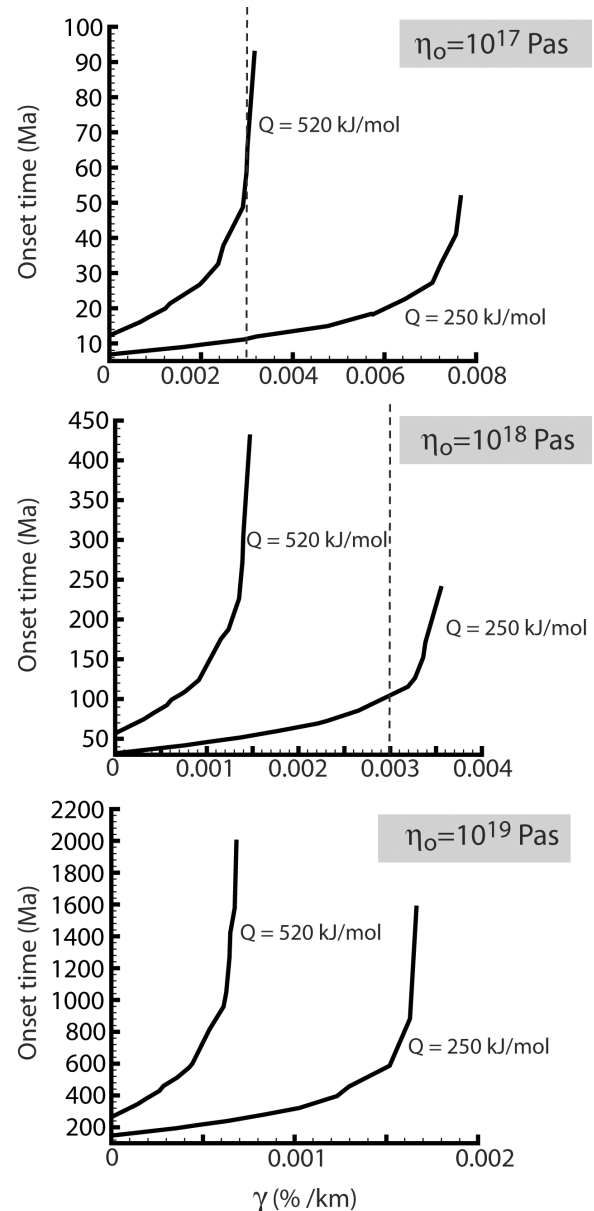


Fig. 10. Onset times and depths for convection in the stably stratified upper mantle after overturn, initiated by the cold upper boundary condition. The results are from analysis in Zaranek and Parmentier (2003). Gamma is the density gradient in stably stratified cumulates, in percent per km. The density gradient in these models is about 0.003, marked with a vertical dashed line. Initial viscosity and activation energy are the critical parameters; if initial viscosity is less than about 10^{19} Pas and activation energy is less than 520 kJ/mol, convection will occur within about 120 Myr after overturn and extend to a depth of about 500 km in the martian mantle.

attendant short-lived magnetic field. The first, and largest, opportunity is overturn placing cold cumulates at the core-mantle boundary. The juxtaposition of cold cumulates with the hot core creates a steep temperature gradient and, therefore, high conductive heat flow. If the core segregated from the magma ocean, the core temperature may be

comparable to the silicate solidus at the core-mantle boundary. Temperature profiles across the core-mantle boundary after overturn are markedly different for the simple fractional crystallization and garnet segregation models. In the simple fractional crystallization model, the coldest, uppermost cumulates fall to the core-mantle boundary and create a temperature difference across the boundary of about 900°C. In the garnet segregation model, relatively warm garnet from the mid-mantle falls to the core-mantle boundary, creating a temperature difference of only about 300°C. A second opportunity for high core-mantle heat flow may be provided by convective instabilities in the overturned mantle's lowest layers. However, stable stratification in the mantle may inhibit the onset of convection.

CONCLUSIONS

The simple models presented in this paper are able to describe to first order a number of aspects of martian evolution:

1. The ages of differentiation of SNC meteorite mantle reservoirs are consistent with fast magma ocean crystallization and overturn to a stable configuration.
2. The garnet segregation model effectively sequesters alumina in Mars' deep mantle, explaining the low Al₂O₃ and high FeO content of the SNC reservoirs relative to bulk silicate Earth and chondritic meteorites.
3. The mantle reservoirs defined at ~4.4 Ga during crystallization and subsequent overturn may remain largely intact, explaining the isotopic heterogeneity of SNCs.
4. Stable stratification after overturn may inhibit the development of thermal convection, thus, preserving these early formed isotopic reservoirs.
5. The planet's moment-of-inertia factor is reasonably reproduced by the overturned models, allowing that significant compositional stratification may persist to the present day.
6. Overturn allows melting of a fraction of the cumulate stratigraphy through decompression and may be the source of an early basaltic crust.
7. By bringing cold material from nearer the planet's surface to the core-mantle boundary, conductive heating of cold, stably stratified mantle near the core-mantle boundary provides a mechanism for early, strong magnetic field generation and cessation.

Acknowledgments—The authors thank K. Righter, V. S. Solomatov, and F. Spera for thorough and constructive reviews, which helped clarify and improve the paper.

Editorial Handling—Dr. Kevin Righter

REFERENCES

- Abe Y. 1993. Physical state of very early Earth. *Lithos* 30:223–235.
- Abe Y. 1997. Thermal and chemical evolution of the terrestrial magma ocean. *Physics of the Earth and Planetary Interiors* 100: 27–39.
- Abe Y. and Matsui T. 1985. The formation of an impact-generated H₂O atmosphere and its implications for the thermal history of the Earth. *Journal of Geophysical Research* 90:C545–C559.
- Abe Y., Ohtani E., Okuchi T., Righter K., and Drake M. 2000. Water in the early Earth. In *Origin of the Earth and Moon*, edited by Canup R. M. and Righter K. Tucson: University of Arizona Press. pp. 413–433.
- Acuña M. H., Connerney J. E. P., Ness N. F., Lin R. P., Mitchell D., Carlson C. W., McFadden J., Anderson K. A., Rème H., Mazelle C., Vignes D., Wasilewski P., and Cloutier P. 1999. Global distribution of crystal magnetism discovered by the Mars Global Surveyor MAG/ER experiment. *Science* 284:790–793.
- Agee C. B. and Walker D. 1988. Static compression and olivine floatation in ultrabasic silicate liquid. *Journal of Geophysical Research* 93:3437–3449.
- Aharonov E., Whitehead J. A., Kelemen P. B., and Spiegelman M. 1995. Channeling instability of upwelling melt in the mantle. *Journal of Geophysical Research* 100:20433–20450.
- Akaogi M., Tanaka A., Ito E. 2002. Garnet-ilmenite-perovskite transitions in the system Mg₄Si₄O₁₂-Mg₃Al₂Si₃O₁₂ at high pressures and high temperatures: Phase equilibria, calorimetry and implications for mantle structure. *Physics of the Earth and Planetary Interiors* 132:303–324.
- Bertka C. M. and Fei Y. 1997. Mineralogy of the martian interior up to core-mantle boundary pressures. *Journal of Geophysical Research* 102:5251–5264.
- Bertka C. M. and Fei Y. 1998a. Density profile of an SNC model martian interior and the moment-of-inertia factor of Mars. *Earth and Planetary Science Letters* 157:79–88.
- Bertka C. M. and Fei Y. 1998b. Implications of Mars Pathfinder data for the accretion history of the terrestrial planets. *Science* 281: 1838–1840.
- Bina C. R. and Helffrich G. 1994. Phase transition Clapeyron slopes and transition zone seismic discontinuity topography. *Journal of Geophysical Research* 99:15853–15860.
- Blichert-Toft J., Gleason J. D., Télouk P., and Albarede F. 1999. The Lu-Hf isotope geochemistry of shergottites and the evolution of the martian mantle-crust system. *Earth and Planetary Science Letters* 173:25–39.
- Borg L. E., Nyquist L. E., Wiesmann H., and Shih C. Y. 1997. Constraints on martian differentiation processes from Rb-Sr and Sm-Nd isotopic analyses of the basaltic shergottite QUE 94201. *Geochimica et Cosmochimica Acta* 61:4915–4931.
- Borg L. E., Nyquist L. E., Wiesmann H., and Reese Y. 2002. Constraints on the petrogenesis of martian meteorites from the Rb-Sr and Sm-Nd isotopic systematics of the ilherzolithic shergottites ALH 77005 and LEW 88516. *Geochimica et Cosmochimica Acta* 66:2037–2053.
- Bottinga Y. and Weil D. F. 1972. The viscosity of magmatic silicate liquids: A model for calculation. *American Journal of Science* 272:438–475.
- Braginsky S. I. 1975. An almost axially symmetric model of the hydromagnetic dynamo of the Earth, I. *Geomagnetism and Aeronomy* 10:1–8.
- Brandon A. D., Walker R. J., Morgan J. W., Goles G. G. 2000. Re-Os isotopic evidence for early differentiation of the martian mantle. *Geochimica et Cosmochimica Acta* 64:4083–4095.

- Campbell G. A. and Forgacs G. 1990. Viscosity of concentrated suspensions: An approach based on percolation theory. *Physics Review* 41A:4570–4573.
- Canup R. and Asphaug E. 2001. Origin of the Moon in a giant impact near the end of the Earth's formation. *Nature* 412:708–712.
- Connerney J. E. P., Acuña M. H., Wasilewski P. J., Ness N. F., Rème H., Mazelle C., Vignes D., Lin R. P., Mitchell D. L., and Cloutier P. A. 1999. Magnetic lineations in the ancient crust of Mars. *Science* 284:794–798.
- Daniel I., Cardon H., Fiquet G., Guyot F., and Mezouar M. 2001. Equation of state of Al-bearing perovskite to lower mantle pressure conditions. *Geophysical Research Letters* 28:3789–3792.
- Davies G. F. 1990. Heat and mass transport in the early Earth. In *Origin of the Earth*, edited by Newsom H. E. and Jones J. H. New York: Oxford University Press. pp. 175–194.
- Drake M. J. and Righter K. 2002. Determining the composition of the Earth. *Nature* 416:39–44.
- Dreibus G. and Wänke H. 1985. Mars: A volatile-rich planet. *Meteoritics & Planetary Science* 20:367–382.
- Fabrichnaya O. B. 1999. The phase relations in the FeO-MgO-Al₂O₃-SiO₂ system: An assessment of thermodynamic properties and phase equilibria at pressures up to 30 GPa. *Calphad* 23:19–67.
- Fei Y., Saxena S. K., and Navrotsky A. 1990. Internally consistent thermodynamic data and equilibrium phase relations for compounds in the system MgO-SiO₂ at high pressure and high temperature. *Journal of Geophysical Research* 95:6915–6928.
- Fei Y., Prewitt C. T., Mao H. K., Bertka C. M. 1995. Structure and density of FeS at high pressure and high temperature and the internal structure of Mars. *Science* 268:1892–1894.
- Folkner W. M., Yoder C. F., Yuan D. N., Standish E. M., Preston R. A. 1997. Interior structure and seasonal mass redistribution of Mars from radio tracking of Mars Pathfinder. *Science* 278:1749–1752.
- Franck S. 1992. Olivine flotation and crystallization of a global magma ocean. *Physics of the Earth and Planetary Interiors* 74: 23–28.
- Frost D. J. and Langenhorst F. 2002. The effect of Al₂O₃ on Fe-Mg partitioning between magnesiowüstite and magnesium silicate perovskite. *Earth and Planetary Science Letters* 199:227–241.
- Halliday A. N., Wanke H., Birck J. L., and Clayton R. N. 2001. The accretion, composition, and early differentiation of Mars. *Space Science Reviews* 96:197–230.
- Hama J. and Suito K. 2001. Thermoelastic models of minerals and the composition of the Earth's lower mantle. *Physics of the Earth and Planetary Interiors* 125:147–166.
- Head J. W., III and Wilson L. 1992. Lunar mare volcanism: Stratigraphy, eruption conditions, and the evolution of secondary crusts. *Geochimica et Cosmochimica Acta* 56:2155–2175.
- Herd C. D. K., Borg L. E., Jones J. H., Papike J. J. 2002. Oxygen fugacity and geochemical variations in the martian basalts: Implications for martian basalt petrogenesis and the oxidation state of the upper mantle of Mars. *Geochimica et Cosmochimica Acta* 66:2025–2036.
- Hess P. C. 2002. Origin of the martian crust and mantle (abstract #6029). Workshop on Unmixing the SNCs: Chemical, Isotopic, and Petrologic Components of the Martian Meteorites.
- Hess P. C. and Parmentier E. M. 1995. A model for the thermal and chemical evolution of the Moon's interior: Implications for the onset of mare volcanism. *Earth and Planetary Science Letters* 134:501–514.
- Hess P. C. and Parmentier E. M. 2001. Implications of magma ocean cumulate overturn for Mars (abstract #1319). 32nd Lunar and Planetary Science Conference.
- Hofmeister A. M. 1983. Effect of a Hadean terrestrial magma ocean on crust and mantle evolution. *Journal of Geophysical Research* 88:4963–4983.
- Holland T. J. B. and Powell R. 1998. An internally consistent thermodynamic data set for phases of petrological interest. *Journal of Metamorphic Geology* 16:309–343.
- Jones J. H. 1986. A discussion of isotopic systematics and mineral zoning in the shergottites: Evidence for a 180 Myr igneous crystallization age. *Geochimica et Cosmochimica Acta* 50:969–977.
- Kavner A., Duffy T. S., and Shen G. 2001. Phase stability and density of FeS at high pressures and temperatures: Implications for the interior structure of Mars. *Earth and Planetary Science Letters* 185:25–33.
- Kelemen P. B. 1990. Reaction between ultramafic rock and fractionating basaltic magma I. Phase relations, the origin of calc-alkaline magma series, and the formation of discordant dunite. *Journal of Petrology* 31:51–98.
- Kelemen P. B., Dick H. J., and Quick J. E. 1992. Formation of harzburgite by pervasive melt rock reaction in the upper mantle. *Nature* 358:635–641.
- Kleine T., Munker C., Mezger K., and Palme H. 2002. Rapid accretion and early core formation on asteroids and the terrestrial planets from Hf-W chronometry. *Nature* 418:952–955.
- Lee D. C. and Halliday A. N. 1995. Hafnium-tungsten chronometry and the timing of terrestrial core formation. *Nature* 378:771–774.
- Lejeune A. M. and Richet P. 1995. Rheology of crystal-bearing silicate melts: An experimental study at high viscosities. *Journal of Geophysical Research* 100:4215–4229.
- Litasov K. and Ohtani E. 2002. Phase relations and melt compositions in CMAS-pyrolite-H₂O system up to 25 GPa. *Physics of the Earth and Planetary Interiors* 134:105–127.
- Longhi J., Knittle E., Holloway J. R., and Wänke H. 1992. The bulk composition, mineralogy, and internal structure of Mars. In *Mars*, edited by Kieffer H. H. et al. Tucson: University of Arizona Press. pp. 184–208.
- Marsh B. D. 1988. Crystal size distribution (CSD) in rocks and the kinetics and dynamics of crystallization I. Theory. *Contributions to Mineralogy and Petrology* 99:277–291.
- Martin D. and Nokes R. 1989. A fluid-dynamic study of crystal settling in convecting magmas. *Journal of Petrology* 30:1471–1500.
- Morgan J. W. and Anders E. 1979. Chemical composition of Mars. *Geochimica et Cosmochimica Acta* 43:1601–1610.
- Morse S. A. 1993. Behavior of a perched crystal layer in a magma ocean. *Journal of Geophysical Research* 98:5347–5353.
- Ohtani E., Yoshihiko N., Suzuki A., Kato T. 1995. Melting relations of peridotite and the density crossover in planetary mantles. *Chemical Geology* 120:207–221.
- Philpotts A. R., Carroll M., Hill J. M. 1996. Crystal mush compaction and the origin of pegmatitic segregation sheets in a thick flood-basalt flow in the Mesozoic Hartford Basin, Connecticut. *Journal of Petrology* 37:811–836.
- Presnall D. C. and Gasparik T. 1990. Melting of enstatite (MgSiO₃) from 10 to 16.5 GPa and the forsterite (Mg₂SiO₄)-majorite (MgSiO₃) eutectic at 16.5 GPa: Implications for the origin of the mantle. *Journal of Geophysical Research* 95:15771–15777.
- Righter K. and Shearer C. K. 2003. Magmatic fractionation of Hf and W: Constraints on the timing of core formation and differentiation in the Moon and Mars. *Geochimica et Cosmochimica Acta* 67:2497–2507.
- Righter K., Hervig R. J., Kring D. A. 1998. Accretion and core formation on Mars: Molybdenum contents of melt inclusion glasses in three SNC meteorites. *Geochimica et Cosmochimica Acta* 62:2167–2177.
- Rubie D. C., Melosh H. J., Reid J. E., Liebske C., Righter K. 2003.

- Mechanisms of metal-silicate equilibration in the terrestrial magma ocean. *Earth and Planetary Science Letters* 205:239–255.
- Schubert G. and Turcotte D. L. 1971. Phase changes and mantle convection. *Journal of Geophysical Research* 76:1424–1432.
- Schubert G. and Spohn T. 1990. Thermal history of Mars and the sulfur content of its core. *Journal of Geophysical Research* 95:14095–14104.
- Schubert G., Yuen D. A., and Turcotte D. L. 1975. Role of phase transitions in a dynamic mantle. *Geophysical Journal of the Royal Astronomical Society* 42:705–735.
- Shaw H. R. 1972. Viscosities of magmatic silicate liquids: An empirical method of prediction. *American Journal of Science* 272:870–893.
- Shih C. Y., Nyquist L. E., Wiesmann H. 1999. Samarium-neodymium and rubidium-strontium systematics of nakhlite Governador Valadares. *Meteoritics & Planetary Science* 34:647–655.
- Shirley D. N. 1986. Compaction of igneous cumulates. *Journal of Geology* 94:795–809.
- Solomatov V. S. 2000. Fluid dynamics of a terrestrial magma ocean. In *Origin of the Earth and Moon*, edited by Canup R. M. and Righter K. Tucson: University of Arizona Press. 555 p.
- Solomatov V. S. and Stevenson D. J. 1993a. Suspension in convective layers and a style of differentiation of a terrestrial magma ocean. *Journal of Geophysical Research* 98:5375–5390.
- Solomatov V. S. and Stevenson D. J. 1993b. Nonfractional crystallization of a terrestrial magma ocean. *Journal of Geophysical Research* 98:5391–5406.
- Solomatov V. S., Olson P., and Stevenson D. J. 1993. Entrainment from a bed of particles by thermal convection. *Earth and Planetary Science Letters* 120:387–393.
- Stevenson D. J. 2001. Mars' core and magnetism. *Nature* 412:214–219.
- Stolper E. M., Walker D., Hager B. H., Hays J. F. 1981. Melt segregation from partially molten source region: The importance of melt density and source region size. *Journal of Geophysical Research* 86:6261–6271.
- Tait S. and Jaupart C. 1992. Compositional convection in a reactive crystalline mush and melt differentiation. *Journal of Geophysical Research* 97:6735–6756.
- Tonks W. B. and Melosh H. J. 1990. The physics of crystal settling and suspension in a turbulent magma ocean. In *Origin of the Earth*, edited by Newsom N. E. and Jones J. H. New York: Oxford University Press. pp. 151–174.
- Tronnes R. G. and Frost D. J. 2002. Peridotite melting and mineral-melt partitioning of major and minor elements at 22–24.5 GPa. *Earth and Planetary Science Letters* 197:117–131.
- Verhoogen J. 1961. Heat balance in the Earth's core. *Geophysical Journal* 4:276–281.
- Wark D. A. and Watson E. B. 2002. Grain-scale channelization of pores due to gradients in temperature or composition of intergranular fluid or melt. *Journal of Geophysical Research* 107, doi: 10.1029/2001JB000365.
- Warren P. H. 1985. The magma ocean concept and lunar evolution. *Annual Review of Earth and Planetary Sciences* 13:201–240.
- Wood J. A., Dickey J. S., Marvin U. B., and Powell B. N. 1970. Lunar anorthosites and a geophysical model of the Moon. Proceedings of the Apollo 11 Lunar Science Conference. pp. 965–988.
- Zaranek S. and Parmentier E. M. Forthcoming. Convective cooling of an initially stably stratified fluid with temperature dependent viscosity. *Journal of Geophysical Research*.
- Zhang J. and Kostak P., Jr. 2002. Thermal equation of state of magnesiowustite ($Mg_{0.6}Fe_{0.4}O$). *Physics of the Earth and Planetary Interiors* 129:301–311.
- Zuber M., Solomon S. C., Phillips R. J., Smith D. E., Tyler G. L., Aharonson O., Balmino G., Banerdt W. B., Head J. W., Johnson C. L., Lemoine F. G., McGovern P. J., Neumann G. A., Rowlands D. D., and Zhong S. 2000. Internal structure and early thermal evolution of Mars from Mars global surveyor topography and gravity. *Science* 287:1788–1793.
-